Co-published by
Institute of Fluid-Flow Machinery
Polish Academy of Sciences
Committee on Thermodynamics and Combustion
Polish Academy of Sciences

http://www.imp.gda.pl/archives-of-thermodynamics/

Novel design and energy analysis of hybrid system activated by low-grade thermal energy conversion

Youcef Maalem[a], Hakim Madani[b*]

[a]Ecole Nationale Polytechnique de Constantine, BP 75, A, Nouvelle ville RP, 25000 Constantine, Algeria
[b]University of Batna 2, Faculty of Technology, Department of Mechanical Engineering, Rue Chahid Boukhlouf M. El Hadi, 05000 Batna, Algeria
*Corresponding author email: h.madani@univ-batna2.dz

Received: 04.08.2025; revised: 08.12.2025; accepted: 23.01.2026

Abstract

A novel power-cooling system triggered by low-grade thermal energy is proposed and studied in this paper. The power-cooling unit combined the engine (organic Rankine cycle) and cooler (ejector-expansion refrigeration cycle employing a booster). Both cycles employ isobutene (R600a) as a working fluid and share a single condenser unit. The performance characteristics (overall coefficient of performance and working fluid mass flow rate per kW of cooling capacity) of the novel unit was investigated using thermodynamic analysis in comparison to the traditional unit that is commonly used. The latter combines the engine (organic Rankine cycle) with the cooler (vapour compression refrigeration cycle) in various operational conditions, including exit temperatures of a boiler unit (60−90°C), a condenser unit (30−55°C) and an evaporator unit (−15−15°C). It was discovered that in comparison to the traditional unit, the novel unit exhibited lower working fluid mass flow rate per kW of cooling capacity and higher overall coefficient of performance. The overall coefficients of performance for both systems increase by 0.5385 and 0.4476, respectively, when the boiler unit's temperature reaches 90°C and the other input specifications are set to typical values. On the other hand, the working fluid mass flow rate per kW cooling capacity of both systems drops by 0.0096 and 0.0064, respectively. Overall, the study demonstrates that the novel system triggered by low-grade thermal energy can be an alternative to the traditional system.

Keywords: Combined system; Working fluid; Expansion ratio; Compression ratio; Performance indicators

Vol. 47(2026), No. 1, 237–253; doi: 10.24425/ather.2026.158673

Cite this manuscript as: Maalem, Y, & Madani, H. (2026). Novel design and energy analysis of hybrid system activated by low-grade thermal energy conversion. *Archives of Thermodynamics*, 47(1), 237–253.

1. Introduction

With rising worldwide energy demands and developments in energy technologies, experts are concentrating on resource optimisation. As a result, there is growing interest in research on the generation and effective use of energy from natural sources like waste heat [1] or biomass [2], geothermal [3], thermal solar [4], etc. In this regard, one of the most promising pieces of equipment in energy engineering is thermodynamic machinery, which uses thermal energy from the aforementioned low-temperature heat source applications to activate cycle performances [5].

The search for environmentally friendly working fluids with high-energy efficiency [6], as well as the design of thermodynamic machinery combination cycles to improve cycle performance through efficient modification [7], are two increasingly popular topics in energy engineering [8].

The hybrid power-cooling system, which combines the organic Rankine cycle (ORC) with the most common cooling cycle, the vapour compression refrigeration cycle (VCRC), is one of the most promising combination cycles. It employs a low-boiling-point working fluid to convert heat input from a variety of low-grade energy sources into usable cooling or power energy [9–12]. Recently, several researchers have used an ORC to produce cooling as a power source for VCRC.

Nomenclature

c – velocity, m/s
CMR – compression ratio in the compressor
COP – coefficient of performance
dp – pressure drop, kPa
EPR – expansion ratio in expander
GWP – global warming potential
h – specific enthalpy, kJ/kg
m – mass flow rate, kg/s
MkW – working fluid mass flow rate per kW of cooling capacity, kg/(s kW)
P – pressure, kPa
Q_{boil} – boiler heat input, kW
Q_{evap} – evaporator cooling capacity, kW
s – specific entropy, kJ/(kg K)
T – temperature, °C
v – specific volume, m^3/kg
W_{comp} – compressor work input, kW
W_{exp} – expander work output, kW
W_{net} – net work output, kW
W_{pump} – pump power consumption, kW
$W_{booster}$ – booster compressor work input, kW
x – vapour quality

Greek symbols

β_{pr} – booster pressure ratio
η – isentropic efficiency
η_{ORC} – power cycle thermal efficiency
μ – entrainment ratio of ejector
ρ – density, kg/m^3

Subscripts

1,...,14 – numbering of states in thermodynamic cycles (ORC, VCRC and EERCIWB)
b – boiler process
boil – boiler
c – condensing process
comp – compressor
cond – condensation
d – diffusor
e – evaporation process
evap – evaporation
exp – expander
is – isentropic process
mn – motive nozzle
ms – mixing section
oval – overall
pf – primary flow
sf – secondary flow
sn – suction nozzle

Abbreviations and Acronyms

EERCIWB – ejector-expansion refrigeration cycle improved by a booster
ORC – organic Rankine cycle
VCRC – vapour compression refrigeration cycle

In the study of Aphornratanaa and Sriveerakul [13], the authors disclosed a simulation examination on a combined engine (ORC) – cooler (VCRC) using two substances, R22 and R164a, as a working fluid. They discovered the computed coefficient of performance values between 1.1 and 1.3 for these fluids, respectively.

The ORC-VCRC system combines steam compression refrigeration with an organic Rankine cycle. Mole et al. [14] studied a combination ORC-VCRC system under various operating conditions that was activated by low-temperature heat sources and used eco-friendly working fluids with R134a for the power and cooling cycles. Their analysis, evaluating working fluids like R1234yf, R1234ze(E) and R1336mzz(Z), was driven by the need for low global warming potential (GWP) alternatives. Quantitatively, they reported that the system could achieve a net power output of up to 45 kW and a cooling capacity of up to 52.5 kW under specific conditions. They concluded that R1336mzz(Z) and R1234ze(E) are the best candidates for the ORC-VCRC system, with R1336mzz(Z) providing the highest exergetic efficiency of approximately 34.3%.

After testing and assessing the ORC-VCRC system for four hydrocarbons (HCs) (propylene (R1270), butane (R600), propane (R290) and isobutane (R600a), Li et al. [15] determined that butane was the optimum working fluid for the ORC-VCRC system, with an overall coefficient of performance (COP) of 0.470. This evaluation was based on a boiler temperature of 90°C, a condensation temperature of 35°C, and an evaporation temperature of 5°C.

Asim et al. [16] looked at the working fluid selection and performance of a VCRC-ORC system, which recovers the waste heat rejected by the air conditioning system's condenser. The R600a-R123 was selected as the fluid pair for the integrated system based on thermodynamics (energy and exergy) and thermo-economic analysis, where the authors found that the system's combined COP could be raised from 3.10 to 3.54. This performance improvement of 14.2% was achieved by utilising a heat source temperature of 85°C.

Saleh [17] proposed using novel hydrofluoroolefins and common hydrofluorocarbons as working fluids in an ORC-VCRC system driven by low-grade thermal energy. The parametric study, evaluating fluids like R1234ze(E), R1234yf, R600 and R600a, identified R600 as optimal due to its superior thermodynamic properties. With a maximum overall performance of 0.718 at a condenser temperature of 30°C and basic values for the remaining parameters, the results demonstrated that working fluid R600 was the best choice compared to the other substances suggested for the hybrid (ORC-VCRC) system. Nonetheless, its flammability should demand enough attention.

The performance of a stand-alone cooling system made up of a cascade refrigeration system and a combined organic Rankine cycle (ORC-CRS), using NH_6/CO_2 for the cascade refrigeration system and toluene for the organic Rankine cycle, was examined by Lizarte et al. [18]. The system was designed for simultaneous refrigeration at two temperature levels: –30°C and 5°C, utilising a low-grade heat source. The highest overall COP value they calculated was 1.70, which significantly outperforms

conventional systems and demonstrates the efficacy of this advanced cascade configuration.

A combined ORC-VCRC system using R600, R600a, R245fa, and pentane as working fluids was theoretically analysed by Cihan [19]. According to the results, the combined system is best suited for R601 fluid.

Bu et al. [20] investigated six working fluids (R134a, R123, R245fa, R290, R600a and R600) to determine the optimal working fluids for an ORC-VCRC system powered by geothermal energy. Their analysis for air-conditioning applications, using a geothermal source at 100°C, showed that R600a provided the best overall performance. Quantitatively, it achieved a maximum overall COP of 0.41 and produced a net power output of 12.5 kW alongside a cooling capacity of 26.7 kW. They decided that R600a was the best option. Nonetheless, the flammability of R600a should be carefully considered.

Wang et al. [21] studied an ORC-VCRC system using two different working fluids for the organic Rankine cycle and conventional vapour compression cycle, namely R245fa and R134a, respectively. The investigation utilised a 6 kW boiler as the heat source. Under a heat source temperature of 120°C, the system achieved a cooling capacity of 5.27 kW, with the ORC subsystem attaining a thermal efficiency of 8.5%. The overall system coefficient of performance reached nearly 0.50, thereby validating the technical feasibility of the dual-fluid, combined cycle for converting low-grade heat into useful cooling.

In Yue et al.'s study [22], an ORC in conjunction with a car air conditioning system using cyclopentane, pentane, R134a and R245fa as working fluids was tested. The system was designed to recover waste heat from a truck engine's exhaust (around 200°C). Their thermo-economic analysis showed that R134a provided the lowest electricity production cost of 0.195 $/kWh and achieved a net power output of 7.8 kW under these conditions. They concluded that, given the operating conditions included in this study, R134a had the best thermal and economic performance when compared to the other working fluids.

The combined ORC-VCRC thermodynamic model was developed by Hu et al. [23] for ship air conditioning in order to effectively use cooling water and transfer waste heat from flue gases. Using five widely used working fluids (R22, R141b, R236ea, R218 and R601), the system performance was examined. Their analysis, based on a flue gas temperature of 350°C, demonstrated that R601 (pentane) achieved the highest exergy efficiency of 35.18% and the largest net power output of 122.9 kW.

Khatoon et al. [24] investigated the thermal performance of an ORC-VCRC system with a common shaft. The organic Rankine cycle used two refrigerants, R245fa and propane, whereas the vapour compression cycle used three: R245fa, R123 and R134a. The system was analysed for a heat source temperature of 120°C, targeting a cooling capacity of 5 kW. Under these conditions, the optimal fluid pair (propane-R123) also produced a net power output of 1.23 kW. At 40°C, propane was used as a working fluid in the organic Rankine cycle and R123 as a working fluid in the vapour compression cycle, yielding the greatest efficiency of 16.48% and a coefficient of performance of 2.85.

Eight working fluids (propane, ammonia, butane, isobutene, propane and R142a) were used in an ORC-VCRC system that was activated by low-grade sensible energy, according to Kim and Perez-Blanco's analysis [25]. The fluids were arranged in order of critical temperature. The study focused on a heat source temperature of 150°C. The results quantified that isobutene (R600a) achieved the highest overall system efficiency of 28.5% and a net power output of 18.3 kW.

Three distinct refrigerants (R123, R134a and R245ca) were assessed by Jeong and Kang [26] in order to determine which was the best fit for the ORC-VCR system. Their analysis for a system utilising a 90°C heat source and a 30°C condenser temperature showed that R123 achieved a thermal efficiency of 9.8% for the ORC and a COP of 4.2 for the VCRC.

Based on thermodynamics (energy and exergy), Egrican and Karakas [27] investigated an ORC-VCRC system with refrigerants R114 for the Rankine cycle and R22 for the vapour compression cycle. Their analysis of the system revealed a significant total exergy destruction of 68%, with the boiler identified as the primary contributor, responsible for over 40% of these losses. The system's overall energy efficiency was reported at approximately 20%. They concluded that it is vital to have as little irreversibility as feasible in the system in order to execute the task more cheaply and efficiently with natural resources.

González et al. [28] developed a rigorous model using the Helmholtz energy function to optimise VCRC-ORC systems, identifying pentane and R1233zd(E) as the best-performing fluids. Their analysis for a heat source temperature of 150°C demonstrated that R1233zd(E) achieved a superior overall system efficiency of 34.5% and an optimal COP of 0.48, outperforming pentane, which reached an efficiency of 32.1%. The study quantified that a 5°C increase in condenser temperature could lead to a system efficiency drop of up to 8%.

Bin Hu and Wang [29] studied methods to reduce greenhouse gas emissions, highlighting vapour compression heat pumps for waste heat recovery. Their comprehensive review of 17 low-GWP working fluids identified isobutene and propane as top performers for standard heat pump applications, achieving high heating capacities and COP comparable to traditional high-GWP fluids like R134a. For high-temperature industrial heat pumps, refrigerants like R1336mzz(Z) and R718 (water) were found to be suitable, capable of achieving temperatures up to 150°C. Quantitatively, systems using R600a demonstrated heating COP ranging from 2.5 to 5.5, depending on operating conditions, while natural working fluids like CO_2 were highlighted for their efficiency in applications requiring a large temperature glide. This review provides crucial application guidelines to facilitate the transition towards environmentally friendly refrigerants in heat pump technology.

Maalem and Madani [30] screened fourteen low-GWP working fluids for a solar-powered ORC-VCRC air conditioning system. Their thermodynamic analysis, based on a heat source temperature of 120°C, demonstrated that the natural working fluid RE170 (dimethyl ether) provided the best overall performance. Quantitatively, RE170 achieved the highest combined system COP of 0.198 and a superior solar system total efficiency of 16.4%, outperforming other candidates like R600a and R290.

A thorough review of the literature on using an organic Rankine cycle to generate cooling as a power source for a vapour

compression refrigeration cycle revealed that, in recent years, a large number of research studies have been conducted to evaluate their performance, with the majority of studies focusing on how well they perform in comparison to various working fluids and/or working conditions.

On the other hand, due to the lower COP of VCRCs, research and development into increasing the cooling performance of the VCRC system through various cycle adjustments has recently received considerable attention in the field of refrigeration engineering [31]. This is because, from a thermodynamics standpoint, employing standard expansion devices (such as capillary tubes, throttle valves, etc.) that use the isenthalpic process reduces the COP of the VCRC due to the high irreversibility in the throttling process. In order to recover this thermodynamic loss, academic experts have conducted numerous studies to identify new ways to increase the cycle performance of the VCRC and recover its energy losses. Ejectors have attracted significant attention as a method for reducing these expansion losses. A two-phase ejector cycle is considered one of the most effective expansion methods for improving the energy efficiency of the refrigeration cycle through a reduction in the expansion loss [32,33]. In this context, our research group has published multiple studies on this topic, including works [34–40].

In the present work, a novel configuration of a power-cooling system ORC-EERCIWB is proposed, in which an ejector-expansion refrigeration cycle with booster compressor (EERCIWB) is employed to enhance the performance of the standard power-cooling system (ORC-VCRC). To the best of our research group's knowledge and by surveying the mentioned literature reviews, such a modification for performance improvement of a standard power-cooling system has not been investigated to date. Therefore, the present study proposes an energy analysis of the proposed power-cooling system.

The energy analysis of the proposed system is carried out and compared with that of the standard power-cooling system (ORC-VCRC) using the same working fluid R600a and various operating conditions. The energy analysis has been performed to investigate the system thermodynamic performances, in particular the performance indicators: overall coefficient of performance (COP_{oval}) and working fluid mass flow rate per kW cooling capacity (MkW), by comparing it with the conventional ORC-VCRC system under boiler exit temperatures (T_{boil}) of 60°C to 90°C, condenser temperatures (T_{cond}) of 30°C to 55°C and evaporator temperatures (T_{evap}) of −15°C to 15°C.

The basic physical and environmental properties of the working fluid used in the investigation are shown in Table 1 [30,35].

Table 1. Basic physical and environmental properties of the working fluid (R600a) used in the investigation.

Specifications	Isobutene
Chemical formula	Iso-C_4H_{10}
Type of working fluid	Hydrocarbon
Standardized international designation	R600a
Molecular structure	
CAS Registry Number	75-28-5
Chemical structure	
Molar mass (kg/kmol)	58.122
Critical temperature (K)	407.85
Critical pressure (MPa)	3.6400
Normal boiling point (K)	261.4
Ozone depletion potential	0
Global warming potential	3

2. Description of power-cooling systems

2.1. ORC-VCRC system

The configuration of the hybrid ORC-VCRC system, which consists of two main thermodynamic cycles, is schematically illustrated in Fig. 1a. The first cycle is the organic Rankine cycle (ORC), designated as (1-2-3-4), and the second cycle is the vapour compression refrigeration cycle (VCRC), designated as (5-6-3-7). The ORC includes a feed pump, boiler unit, expander unit and condenser unit, while the VCRC includes a compressor unit, condenser unit, throttle valve and evaporator unit. This kind of configuration uses a low-temperature heat source as a heat input to power the hybrid system, which has a shaft connecting the compressor of the vapour compression refrigeration cycle and the expander of the organic Rankine cycle.

These four fundamental transformations of the hybrid system occur during each thermodynamic cycle, and the condensation processes of both the organic Rankine cycle (ORC) and the vapour compression refrigeration cycle (VCRC) take place in a shared condenser at the same pressure.

The different processes of the combined systems (ORC and VCRC) are presented as follows:

In the ORC:

- process (1→2s) − is an isentropic expansion process across the expander;
- process (1→2) − is the actual expansion process;
- process (2→3) − is a heat rejection (condensation) process across the condenser;
- process (3→4s) − is an isentropic pumping process;
- process (3→4) − is the actual pumping work;
- process (4→1) − is a heat addition process in the boiler.

In the VCRC:

- process (5→6s) − is an isentropic compression in the compressor;
- process (5→6) − is the actual compression process in the compressor;
- process (6→3) − is a heat rejection (condensation) process across the condenser;
- process (3→7) − is an isenthalpic expansion across the throttle valve;
- process (7→5) − is a heat absorption (evaporation) in the evaporator.

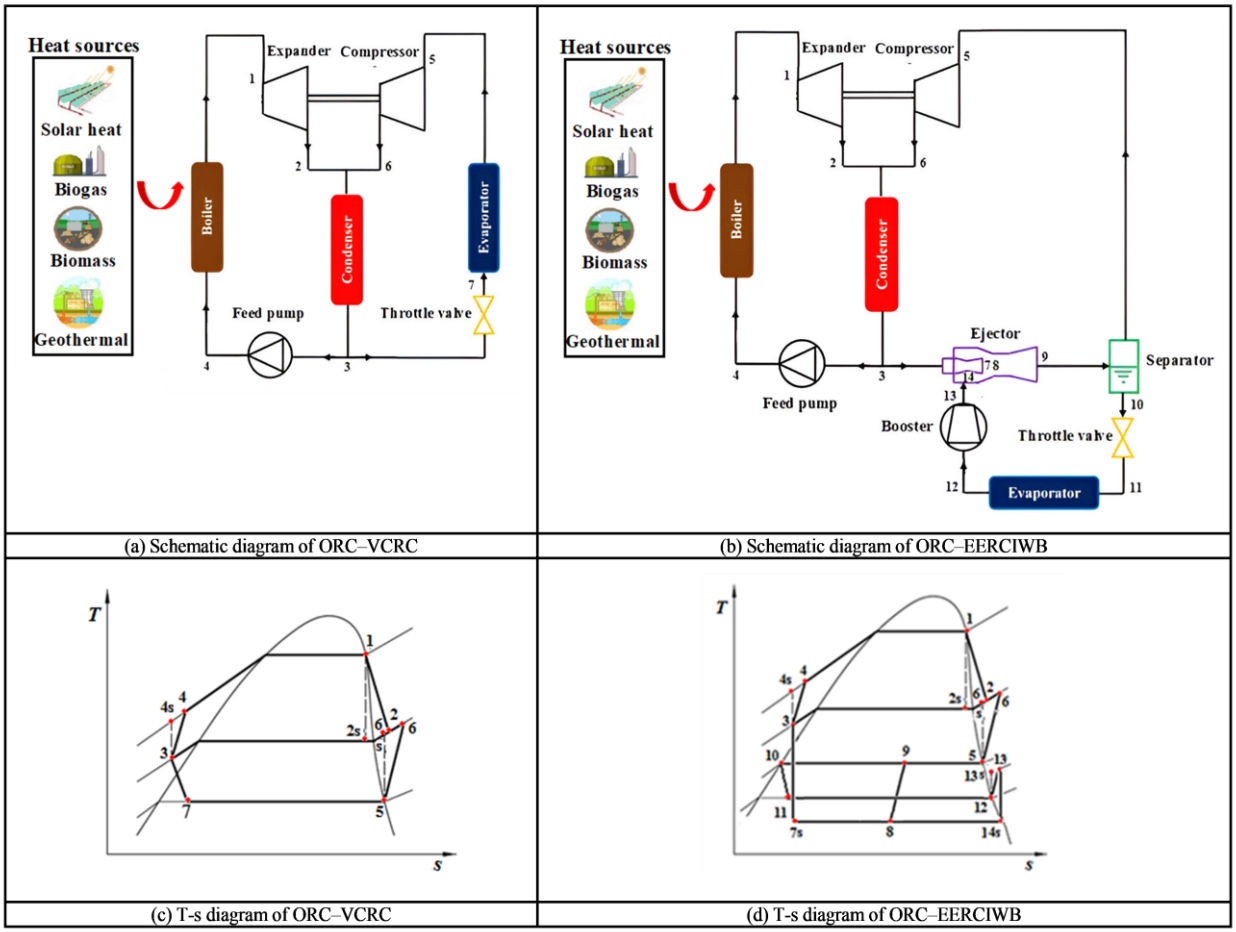

Fig. 1. Schematic illustrations (a, b) and *T*–*s* diagrams (c, d) of power-cooling systems.

The same refrigerant is used in the hybrid ORC-VCRC system's two thermodynamic cycles (ORC and VCRC), which operate in the following ways, respectively:

In the ORC: The heat absorbed from the low-temperature heat source causes the working fluid in the boiler to heat and evaporate at state 4. Next, the expander receives the high-pressure working fluid steam (state 1), whose enthalpy is transformed into power. After that, the working fluid enters the condenser (state 2), where the heat rejection from the external medium causes the condenser to condense at the condensation temperature. To complete the thermodynamic cycle, the working fluid then enters the feed pump (state 3), which transports it to the boiler. Lastly, the thermodynamic cycle's compressor (VCRC) is powered by the thermodynamic cycle's net mechanical power (ORC).

In the VCRC: In the compressor at state 5, the working fluid is compressed to high pressure (state 6). Then, the working fluid enters the condenser, where it condenses at the condensation temperature due to the heat rejection (condensation process) to the condensing medium. Next, the working fluid enters the throttle valve, where it expands at state 7. Finally, in the evaporator, the working fluid absorbs the cooling load from the cooling space at the VCRC evaporation temperature.

2.2. Proposed ORC-EERCIWB system

Figure 1b provides a schematic illustration of the cycle configuration for the suggested hybrid ORC-EERCIWB system. In contrast to the traditional hybrid ORC-VCRC system, the ORC (1-2-3-4) features an ejector-expansion refrigeration cycle improved by a booster circuit connected to its main circuit, which is designated as (5-6-3-7-8-9-10-11-12-13-14). The EERCIWB is made up of different components than the VCRC; it consists of a compressor, condenser, throttle valve, two-phase ejector, gas–liquid separator, booster and an evaporator. The ORC contains the same components as the ORC of the conventional hybrid system ORC-VCRC.

Such as a conventional hybrid ORC-VCRC system, a heat input from a low-temperature heat source drives the proposed hybrid system, where the compressor of the EERCIWB and the expander of the ORC are directly attached through a shaft.

Figure 1d shows the proposed system's temperature-entropy (*T*–*s*) diagram. The subsystems (ORC and EERCIWB) in this proposed system both use the same working fluid, and subsystem condensation occurs in a common condenser at the same pressure.

The following are the different processes that characterise the EERCIWB of the suggested combined ORC-EERCIWB system:

- process (9→5) − send the vapour of the mixture to the compressor;
- process (9→10) − send the liquid portion to the throttle valve;
- process (5→6s) − is an isentropic compression across the compressor;
- process (5→6) − is the actual compression process in the compressor;
- process (6→3) − is a heat rejection (condensation) process across the condenser;
- process (3→7s) − is an ideal expansion process throughout the motive nozzle;
- process (13→14s) − is an ideal process in the suction nozzle;
- process (7→8) − is a mixing process in the mixing section at constant pressure;
- process (8→9) − is a compression process of mixing in a diffuser section;
- process (10→11) − is an isenthalpic expansion across the throttle valve;
- process (11→12) − is a heat absorption (evaporation) in the evaporator;
- process (12→13) − is the actual compression process in the booster;
- process (12→13s) − is an isentropic compression across the booster.

The thermodynamic cycle EERCIWB of the proposed combined system works as follows:

The saturated liquid leaving the condenser (state 3) expands in the ejector's motive nozzle, causing its pressure to drop dramatically at state point 7. As a result, the suction nozzle directs the secondary flow (state 13) into the ejector device, where the pressure at the exit (state 14) equals that of state point 7. In the ejector's mixing section, the two streams are continuously mixed to create stream 8, which is released at the end of the section. When this stream reaches the diffuser, its pressure rises and its velocity falls, creating a two-phase flow (state 9). The vapour portion of the two-phase flow enters the compressor unit, where it is forced to rise in pressure (state 6) and travels to the condenser unit after being separated in a vapour-liquid separator. When the saturated liquid exits the separator at state point 10, the throttling valve reduces it until it reaches the evaporator's pressure and temperature (state 11). Cooling occurs when heat from a cooled medium is absorbed and evaporated by the stream passing through the evaporator. As the saturated vapour exits the evaporator (state 12), it enters the booster compressor and accumulates pressure until it reaches the ejector's secondary flow (state 13).

3. Mathematical models and computational procedures

3.1. Thermodynamic assumptions

Based on previously published literature [15,41,42], the following thermodynamic assumptions form the foundation for the modelling and analysis of both systems in this study:

- The systems are working under steady state conditions.
- Pressure losses in the pipelines and through the heat exchangers are disregarded.
- The system's constituent parts are adiabatic.
- The kinetic energy and potential energies of operating modes are neglected in all sub-systems.
- The working fluid at the exit of the boiler is assumed to be saturated.
- At the evaporators' exit of the subsystems (VCRC and EERCIWB), the working fluid is in the saturated vapour state.
- To prevent cavitation in the boiler feed pump, the working fluid is subcooled to 3°C at the condenser exit of the subsystems (ORC, VCRC and EERCIWB).
- The throttling process in the throttle valve is isenthalpic.
- The vapour stream from the separator is a saturated vapour, and the liquid stream from the separator is a saturated liquid.
- The transformations in all heat exchangers are isobaric processes.
- The compressors are working with an appropriate value of isentropic efficiency.
- The ejector's flow dynamics were modelled as a 1D homogeneous equilibrium.
- The kinetic energy of the flow streams at the ejector inlet and outlet is negligible.
- The mixing pressure in the mixing chamber of the ejector is constant.
- In ejector modelling, the friction losses inside the ejector are taken into account using appropriate values for nozzle, diffuser and mixing section efficiencies.
- The efficiencies of the ejector remain constant.
- The net power produced by the ORC is the power consumed by the compressor of the VCRC and EERCIWB.

3.2. Theoretical models

To simulate the thermodynamic performance of the combined refrigeration and power systems (ORC-VCRC and ORC-EERCIWB), the first stage in the modelling method is to compute the required thermodynamic parameters (such as pressure, enthalpy, entropy, etc.) of R600a at the outlets of each component of the thermodynamic cycles, as defined in Fig 1. This is done prior to modelling the considered thermodynamic cycles.

The Coolprop library, implemented in Matlab, was employed to determine the thermodynamic properties of the working fluid in the present study. The following thermodynamic models are used to calculate the thermodynamic properties (such as pressure, enthalpy, entropy, etc.) of the subcycles ORC, VCRC and EERCIWB, based on the operating conditions (such as boiler temperature, condenser temperature, evaporator temperature, etc.) using Matlab.

The thermodynamic parameters of the state of saturated vapour at the boiler unit outlet of the subcycle ORC are obtained as:

$$P_1 = P(T_{boil}, x = 1), \quad (1)$$

$$h_1 = h(T_{boil}, x = 1), \quad (2)$$

$$s_1 = s(T_{boil}, x = 1), \quad (3)$$

$$\rho_1 = \rho(T_{boil}, x = 1). \quad (4)$$

The specific volume of saturated vapour is determined by

$$v_1 = \frac{1}{\rho_1}. \quad (5)$$

The thermodynamic parameters of the state of saturated vapour at the evaporator unit outlet of the subcycle VCRC are obtained as:

$$P_5 = P(T_{evap}, x = 1), \quad (6)$$

$$h_5 = h(T_{evap}, x = 1), \quad (7)$$

$$s_5 = s(T_{evap}, x = 1). \quad (8)$$

The thermodynamic parameters of the state of subcooled liquid leaving the shared condenser of subcycles (ORC, VCRC and EERCIWB) are obtained as:

$$P_3 = P(T_{cond}, x = 0), \quad (9)$$

$$T_3 = T_{cond} - 3, \quad (10)$$

$$h_3 = h(T_3, P_3), \quad (11)$$

$$s_3 = s(T_3, P_3). \quad (12)$$

At the throttle valve, the throttling process is an isenthalpic process. Therefore, the enthalpy at the outlet of the throttle valve of the subcycle VCRC is calculated as

$$h_7 = h_3. \quad (13)$$

The thermodynamic parameters of the working fluid at the feed pump outlet of the subcycle ORC are obtained as:

$$P_4 = P_1, \quad (14)$$

$$s_4 = s_3, \quad (15)$$

$$h_{4s} = h(P_4, s_4). \quad (16)$$

The actual outlet enthalpy is determined by

$$h_4 = h_3 + \frac{h_{4s} - h_3}{\eta_{pump}}, \quad (17)$$

where η_{pump} refers to the isentropic efficiency of the feed pump. The thermodynamic parameters of the working fluid at the compressor unit outlet of the subcycle VCRC are obtained as:

$$P_6 = P_3, \quad (18)$$

$$s_6 = s_5, \quad (19)$$

$$h_{6s} = h(P_6, s_6). \quad (20)$$

The actual outlet enthalpy is determined by

$$h_6 = h_5 + \frac{h_{6s} - h_5}{\eta_{comp}}, \quad (21)$$

where η_{comp} refers to the isentropic efficiency of the compression process.

The thermodynamic parameters of the working fluid at the expander unit outlet of the subcycle ORC are obtained as:

$$P_2 = P_3, \quad (22)$$

$$s_2 = s_1, \quad (23)$$

$$h_{2s} = h(P_2, s_2). \quad (24)$$

The actual outlet enthalpy is determined by

$$h_2 = h_1 + \frac{h_{2s} - h_1}{\eta_{exp}}, \quad (25)$$

where η_{exp} refers to the isentropic efficiency of the expansion process.

The specific volume of the working fluid at the expander unit outlet of the subcycle ORC is determined by

$$v_2 = \frac{1}{\rho_2}, \quad (26)$$

where

$$\rho_2 = \rho\,(h_2, P_2). \quad (27)$$

The thermodynamic parameters of the state of saturated vapour at the evaporator unit outlet of the subcycle EERCIWB are obtained as:

$$P_{12} = P(T_{evap}, x = 1), \quad (28)$$

$$h_{12} = h(T_{evap}, x = 1), \quad (29)$$

$$s_{12} = s(T_{evap}, x = 1). \quad (30)$$

The thermodynamic parameters of the working fluid at the booster unit outlet of the subcycle EERCIWB are obtained as [41]:

$$P_{13} = P_{12}\beta_{pr}, \quad (31)$$

$$s_{13} = s_{12}, \quad (32)$$

$$h_{13s} = h(P_{13}, s_{13}), \quad (33)$$

where β_{pr} is the booster pressure ratio. The isentropic efficiency of the booster unit is calculated as

$$\eta_{booster} = 0.874 - 0.0135\beta_{pr}. \quad (34)$$

The actual outlet enthalpy is determined by

$$h_{13} = h_{12} + \frac{h_{13s} - h_{12}}{\eta_{booster}}. \quad (35)$$

For the gas-liquid separator outlet of the subcycle EERCIWB, the enthalpy of saturated vapour and the saturated liquid are calculated respectively as:

$$h_5 = h(P_9, x = 1), \quad (36)$$

$$h_{10} = h(P_9, x = 0). \quad (37)$$

At the throttle valve, the throttling process is isenthalpic. Therefore, the enthalpy at the outlet of the throttle valve of the subcycle EERCIWB is calculated as

$$h_{11} = h_{10}. \quad (38)$$

3.2.1. Ejector modelling

The ejector is a critical component in the ORC-EERCIWB system. The effectiveness of the system is determined by the entrainment ratio (μ), which is the mass flow rate ratio between the secondary and primary flows:

$$\mu = \frac{m_{sf}}{m_{pf}}. \quad (39)$$

When modelling an ejector device, two models are typically used to simulate the ejector's performance. These models divide the ejector into two categories, based on where the motive nozzle exit plane is located:

- constant-pressure ejector,
- constant-area ejector.

Both models have been extensively investigated in the past [43], with a number of scholars demonstrating that the constant-pressure ejector outperforms the constant-area ejector and hence is more commonly utilised. Thus, in the current investigation, a constant-pressure ejector is adopted. This paper uses the constant-pressure ejector mathematical model that was used by Maalem et al. [34,36,39]. The motivation nozzle, suction nozzle, mixing section, and diffusion section ejector modelling equations in this model are developed as follows:

At the suction nozzle outlet, the thermodynamic parameters of the primary flow can be calculated as:

$$P_{14} = P_{13} - dp, \quad (40)$$

$$s_{14} = s_{13}, \quad (41)$$

$$h_{14s} = h(P_{14}, s_{14}). \quad (42)$$

The suction nozzle enthalpy is determined from its isentropic relationship and given as

$$h_{14} = h_{13} - \eta_{sn}(h_{13} - h_{14s}). \quad (43)$$

The velocity of the secondary flow at the suction nozzle outlet is determined as

$$c_{14} = \sqrt{2(h_{13} - h_{14})}. \quad (44)$$

At the motive nozzle outlet, the thermodynamic parameters of the secondary flow can be calculated as:

$$P_7 = P_{14}, \quad (45)$$

$$h_{7s} = h(P_7, s_3). \quad (46)$$

The motive nozzle exit enthalpy is determined from its isentropic relationship and given as

$$h_7 = h_3 - \eta_{mn}(h_3 - h_{7s}). \quad (47)$$

The velocity of the motive fluid at the motive nozzle exit is calculated as

$$c_7 = \sqrt{2(h_3 - h_7)}. \quad (48)$$

The two streams coming out of the motive and suction nozzles are mixed at a constant pressure. So, for the mixing section:

$$P_8 = P_7. \quad (49)$$

Applying the momentum and energy conservation on the mixing section would result in relations for its exit velocity and enthalpy:

$$c_8 = \sqrt{\eta_{ms}}[c_7/(1+\mu) + c_{14}\mu/(1+\mu)], \quad (50)$$

$$h_8 = \frac{1}{1+\mu}(h_7 + c_7^2/2) + \frac{\mu}{1+\mu}(h_{14} + c_{14}^2/2) - c_8^2/2, \quad (51)$$

$$s_8 = s(P_8, h_8). \quad (52)$$

The mixed flow is decelerated in the diffuser part, converting kinetic energy back into pressure rise.

Similarly, applying the conservation of energy and the isentropic relation gives the following equations for the diffuser:

$$h_9 = h_8 + \frac{c_8^2}{2}, \quad (53)$$

$$h_{9s} = h_8 + \eta_d(h_9 - h_8). \quad (54)$$

The pressure of the mixture at the ejector exit is determined by the following formula:

$$P_9 = P(h_{9s}, s_8). \quad (55)$$

In the ejector calculations, state 9 is the most important. Previous calculations cannot calculate the vapour quality at the ejector output due to the unknown entrainment ratio. To address this issue, the initial guess value of μ is assumed during the iterative computation procedure. Furthermore, the isentropic efficiencies for the ejector component and operating temperatures are given. To verify the preliminary input value for the entrainment ratio, the results of the two formulas are compared:

$$x_9 = x(h_9, P_9), \quad (56)$$

$$x_9' = \frac{1}{1+\mu}. \quad (57)$$

If the two values match each other, then the assumed μ is maintained; otherwise, another value of μ is chosen, and the loop is started again, as shown in the flowchart displayed in Fig. 2. With all state points defined above, the following key performance indicators are calculated in the next sections to evaluate and compare the systems.

3.2.2. ORC modelling

The governing equations of the organic Rankine cycle are developed as follows [15]:

The expander's output power is calculated using

$$W_{exp} = m_{ORC}(h_1 - h_{2s})\,\eta_{exp}. \quad (58)$$

The required power to the pump can be written as

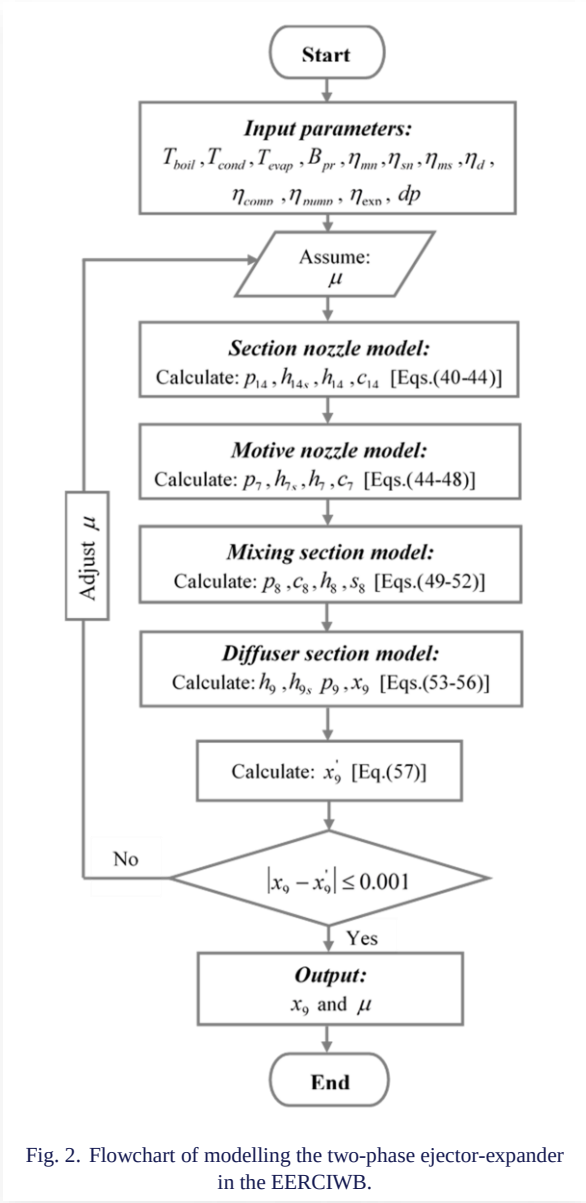

Fig. 2. Flowchart of modelling the two-phase ejector-expander in the EERCIWB.

$$W_{pump} = m_{ORC}\,\frac{h_{4s}-h_3}{\eta_{pump}}. \quad (59)$$

The net output power from the ORC is defined as

$$W_{net} = W_{exp} - W_{pump}. \quad (60)$$

The rate of heat transfer in the boiler can be expressed as

$$Q_{boil} = m_{\mathrm{ORC}}(h_1 - h_4). \quad (61)$$

The expansion ratio across the expander is given by

$$\mathrm{EPR} = \frac{v_2}{v_1}. \quad (62)$$

The thermal efficiency of the ORC is defined as

$$\eta_{\mathrm{ORC}} = \frac{W_{net}}{Q_{boil}}. \quad (63)$$

3.2.3. VCRC modelling

The governing equations of the VCRC are developed as follows:

For the compressor, the input power in the VCRC can be written as [44]:

$$W_{comp,VCRC} = W_{net}. \quad (64)$$

The compression ratio across the compressor is given by

$$\mathrm{CMR} = \frac{P_6}{P_5}. \quad (65)$$

The cooling capacity of VCRC is calculated by

$$Q_{evap,VCRC} = m_{VCRC}(h_5 - h_7), \quad (66)$$

with

$$m_{VCRC} = \frac{W_{comp,VCRC}(h_5 - h_{6s})}{\eta_{comp}}. \quad (67)$$

The COP of the VCRC is given by

$$\mathrm{COP}_{VCRC} = \frac{Q_{evap,VCRC}}{W_{comp,VCRC}}. \quad (68)$$

To characterise the ORC-VCRC system performance, the overall COP and the working fluid mass flow rate per kW cooling capacity are computed using the following two formulas, respectively:

$$\mathrm{COP}_{oval,ORC-VCRC} = \eta_{ORC}\mathrm{COP}_{VCRC}, \quad (69)$$

$$\mathrm{MkW}_{ORC-VCRC} = \frac{m_{ORC}+m_{VCRC}}{Q_{evap,VCRC}}. \quad (70)$$

3.2.4. EERCIWB modelling

The governing equations of the EERCIWB are developed as follows:

For the compressor unit, the input power in the EERCIWB can be written as

$$W_{comp,EERCIWB} = W_{net}. \quad (71)$$

The compression ratio across the compressor is given by

$$\mathrm{CMR} = \frac{P_6}{P_5}. \quad (72)$$

The cooling capacity of EERCIWB can be expressed as

$$Q_{evap,EERCIWB} = m_{sf}(h_{12} - h_{11}), \quad (73)$$

with

$$m_{sf} = m_{pf}\mu, \quad (74)$$

$$m_{pf} = \frac{W_{comp,EERCIWB}}{h_6 - h_5}. \quad (75)$$

For the booster, the input power in the EERCIWB can be written as

$$W_{booster,EERCIWB} = m_{sf}(h_{13} - h_{12}). \quad (76)$$

The COP of the EERCIWB is given by

$$\mathrm{COP}_{EERCIWB} = \frac{Q_{evap,EERCIWB}}{W_{comp,EERCIWB} + W_{booster,EERCIWB}}. \quad (77)$$

Table 2. Relative errors of performance indicators according to [15].

Refrigerant	Indicators	Average relative error (%)	Maximum relative error (%)
R290	COP_{oval}	0.05	0.10
	MkW	0.53	0.83
R600	COP_{oval}	0.04	0.07
	MkW	0.71	1.20
R600a	COP_{oval}	0.04	0.07
	MkW	0.74	1.05
R1270	COP_{oval}	0.10	0.30
	MkW	0.68	0.68

To characterise the ORC-EERCIWB system performance, the overall COP and the working fluid mass flow rate per kW of cooling capacity are computed using the following two formulas, respectively:

$$\mathrm{COP}_{oval,ORC-EERCIWB} = \eta_{ORC}\mathrm{COP}_{EERCIWB}, \quad (78)$$

$$\mathrm{MkW}_{ORC-EERCIWB} = \frac{m_{ORC}+m_{sf}}{Q_{evap,EERCIWB}}. \quad (79)$$

3.3. Conditions of operation for the ORC-VCRC and ORC-EERCIWB computation

The cycles are simulated under a variety of operating conditions in order to compare the thermodynamic performances of the systems ORC-VCRC and ORC-EERCIWB. The following are the given operating conditions [15,34]:

- The working fluid is R600a.
- The temperature of the heat source is 100°C.
- The boiler temperature ranges from 60°C to 90°C.
- The condensation temperature ranges from 30°C to 55°C.
- The evaporation temperature ranges from −15°C to 15°C.
- The working fluid mass flow rate in ORC is 1.0 kg/s.
- The booster pressure ratio is 1.5.
- The isentropic efficiency of the compressor, feed pump and expander is 75%, 75% and 80%, respectively.
- The isentropic efficiency of the motive nozzle, suction nozzle, mixing section and diffusion section is 85%, 85%, 95% and 85%, respectively.

3.4. Model validation

Before presenting the simulation findings, it is appropriate to have a quick discussion about the validation of the system's simulation models.

The proposed hybrid (ORC-EERCIWB) system is a novel power-cooling system design that has not been investigated in any previous studies. As a result, to validate the numerical solution, the established simulation model is solved under the identical operating conditions as those described in [15] for the basic hybrid (ORC-VCRC) system and the same working fluids (R290, R600, R600a and R1270). The effect of boiler temperature is displayed against performance indicators (overall coefficient of performance (COP_{oval}) and working fluid mass flow rate per kW of cooling capacity (MkW), according to [15]. The comparison results are displayed in Fig. 3. The relative error between the present model and the Ref. [15] data was calculated for each data point. The maximum relative errors for each fluid and performance indicators are summarised in Table 2.

The comparison for different boiler temperatures demonstrates an excellent agreement between the results. It is found that the average error for the COP_{oval} is less than 0.11%, peaking at 0.30% for an individual fluid. Similarly, the MkW shows an average error under 0.75% and a maximum of 1.20%. These minimal deviations confirm the validity of our simulation model.

4. Simulation results and discussion

The results are presented with four significant figures to accurately reflect the comparative trends generated by the simulation. The calculations were performed using the Matlab software with built-in high-accuracy refrigerant property databases (Coolprop library). The solver convergence criterion was set to 10^{-6}, ensuring negligible numerical error. The precision of the reported values is therefore representative of the model's internal consistency and is sufficient for the comparative analysis presented.

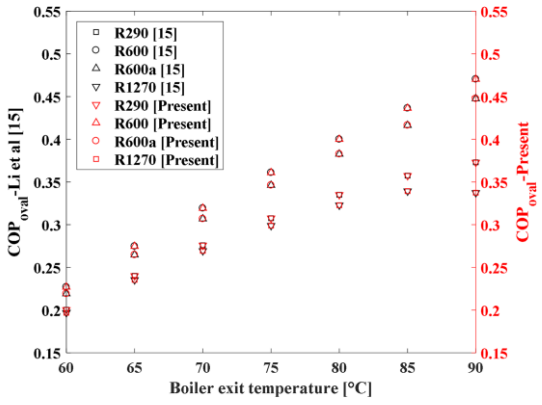

(a)

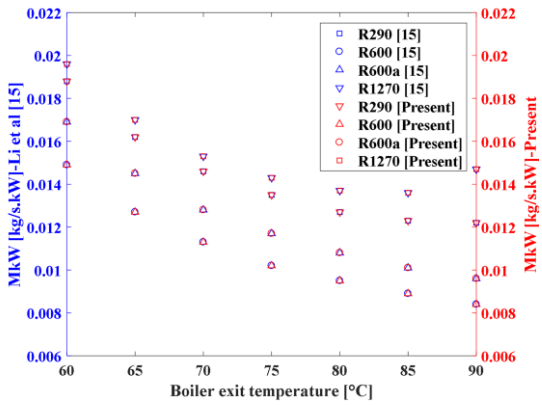

(b)

Fig. 3. Verification of the simulation results of the present work compared with those from [15].

4.1. Effect of boiler temperature on performance indicators

The following Figs. 4−6 show the impact of boiler temperature on ORC-VCRC and ORC-EERCIWB performances using R600a as a working fluid, while maintaining the other parameters constant (T_{cond} = 40°C and T_{evap} = 5°C).

Figure 4 exhibits the evolution of both $COP_{oval\text{-}(ORC–VCRC)}$ and $COP_{oval\text{-}(ORC–EERCIWB)}$ with the boiler exit temperature of the combined refrigeration and power systems (ORC-VCRC and ORC–EERCIWB), respectively. As can be seen from the obtained simulation results, the $COP_{oval\text{-}(ORC–VCRC)}$ and $COP_{oval\text{-}(ORC–EERCIWB)}$ of the two combined systems improve with boiler temperature. Lower boiler exit temperatures (60°C) resulted in lower values of $COP_{oval\ (ORC–VCRC)}$ and $COP_{oval\text{-}(ORC–EERCIWB)}$, but both systems' COP_{oval} increased as the boiler exit temperature rose. This can be explained by the fact that as boiler temperature rises, the amount of heat added to the boiler increases as well, leading to an increase in COP_{oval} values.

It was discovered that the COP_{oval} obtained with the R600a in the ORC-VCRC and ORC-EERCIWB systems was 0.4476 and 0.5385, respectively, with the high boiler exit temperature (90°C). It should be mentioned that when the boiler exit temperature rises from 60°C to 90°C, the COP_{oval} values for the two systems increase from 0.2192 to 0.4476 and from 0.2637 to 0.5385, respectively.

The proposed hybrid ORC-EERCIWB system outperforms the hybrid ORC-VCRC system in terms of COP_{oval}, and the differences between the $COP_{oval\text{-}(ORC–VCRC)}$ and $COP_{oval\text{-}(ORC–EERCIWB)}$ are greater at high boiler exit temperatures than they are at low ones, according to a comparison of the results obtained for the two hybrid systems.

The findings show that, within the boiler temperature range taken into consideration, the COP_{oval} values increase by 20.30% when compared to those of the hybrid (ORC-VCRC) system. It is clear that the ORC-EERCIWB configuration offers a viable way to enhance the efficiency of the traditional ORC-VCRC system for recovering low-grade thermal energy.

Figure 5 illustrates the effects of the boiler exit temperature on the MkW of the combined refrigeration and power systems

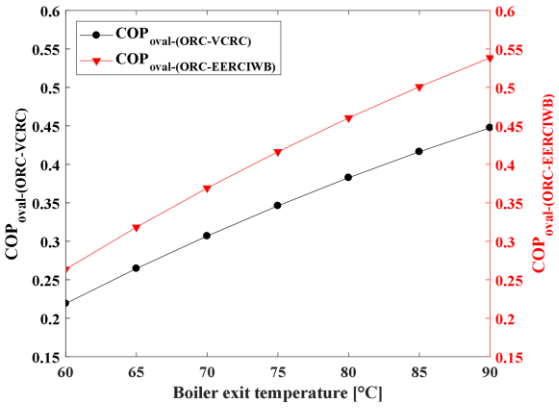

Fig. 4. Effect of boiler temperature on COP_{oval} of the ORC-VCRC and ORC-EERCIWB.

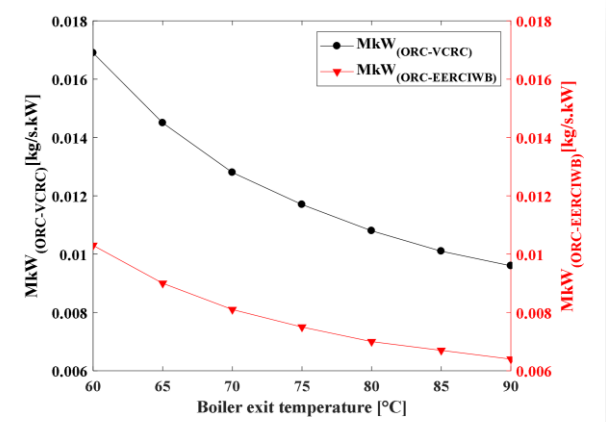

Fig. 5. Effect of boiler temperature on MkW in the ORC-VCRC and ORC-EERCIWB.

using R600a as a working fluid, $MkW_{(ORC–VCRC)}$ and $MkW_{(ORC–EERCIWB)}$, respectively.

The results presented in Fig. 5 demonstrate that the $MkW_{(ORC–VCRC)}$ and $MkW_{(ORC–EERCIWB)}$ generally decrease with boiler exit temperature. Specifically, higher values of $MkW_{(ORC–VCRC)}$ and $MkW_{(ORC–EERCIWB)}$ were observed at lower boiler exit temperatures (60°C); conversely, as boiler exit temperature increased, the MkW of both systems also decreased, which signifies that both investigated systems become more efficient in their use of the R600a to produce cooling. The comparison of simulation results for the two hybrid systems reveals that, within the boiler temperature range considered, the proposed hybrid system ORC-EERCIWB produced the lowest MkW compared to the hybrid system ORC-VCRC. This can be explained by the fact that the ORC-EERCIWB system needs less working fluid mass to deliver the same amount of cooling power as the ORC-VCRC system. Figure 5 shows that when the boiler exit temperature rises from 60°C to 90°C, the MkW values obtained for the two systems using the R600a decrease from 0.0169 to 0.0096 and from 0.0103 to 0.0064, respectively. According to the data, the MkW in the ORC-EERCIWB system is lower than in the ORC-VCRC system by 39.05 % to 33.33 %, leading to a higher COP_{oval}. Furthermore, it is worth noting that the ORC-EERCIWB configuration presents a viable option for lowering the MkW of the traditional ORC-VCRC system in order to recover low-grade thermal energy.

Figure 6 illustrates the effects of the boiler exit temperature on the EPR of both considered combined refrigeration and power systems using the hydrocarbon R600a as a working fluid. The figure indicates that when the boiler exit temperature rises, the EPR rises as well, where it is evident that the minimum EPR is reached at 60°C, while the maximum EPR is reached at 90°C. This rise can be explained by the fact that the saturation pressure of a fluid increases exponentially with its temperature, and the increase in the boiler exit temperature forces both systems to achieve a much higher pressure at the expander inlet. As a result, the EPR rises as well. As the boiler exit temperature rises from 60°C to 90°C, the EPR values obtained for the two systems using the hydrocarbon R600a increase from 1.6850 to 3.4951.

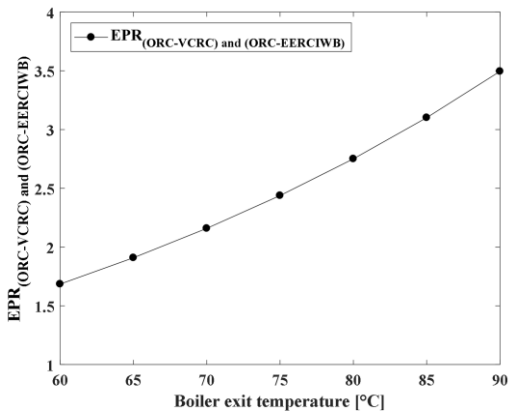

Fig. 6. Effect of boiler temperature on EPR in the ORC-VCRC and ORC-EERCIWB.

4.2. Effect of condensation temperature on the performance indicators

The following Figs. 7–10 show the effect of condensation temperature on the ORC-VCRC and ORC-EERCIWB systems' performances using the hydrocarbon R600a as a working fluid, while maintaining the other parameters constant (T_{boil} = 80°C, T_{evap} = 5°C).

Figure 7 shows the evolution of the $COP_{oval\text{-}(ORC–VCRC)}$ and $COP_{oval\text{-}(ORC–EERCIWB)}$ with the condensation temperature of the combined refrigeration and power systems, respectively. It is evident from looking at the profiles in the figure that the condensation temperature has a significant impact on the COP_{oval} of the two systems, with an increase in condensation temperature leading to a decrease in both $COP_{oval\text{-}(ORC–VCRC)}$ and $COP_{oval\text{-}(ORC–EERCIWB)}$. This is because, while the compressor's inlet temperature and pressure remain constant, the condenser temperature rises at the compressor's outlet, increasing pressure, enthalpy, and resulting in a decrease in COP_{oval} The maximum $COP_{oval\text{-}(ORC–VCRC)}$ and $COP_{oval\text{-}(ORC–EERCIWB)}$ values are reached at low condensation temperatures (30°C), whereas the minimum values are reached at higher condensation temperatures (55°C). It should be noted that when the condensation temperature increases from 30°C to 55°C, the COP_{oval} values for the two systems obtained with the R600a fall from 0.6952 to 0.1562 and from 0.8206 to 0.1966, respectively.

It is clear from a comparison of the suggested hybrid ORC-EERCIWB system's results with those of the hybrid ORC-VCRC system that the proposed hybrid system achieves a higher COP_{oval}. The findings show that when compared to hybrid ORC-VCRC values, the COP_{oval} values increase by 18.03% to 25.86%.

Figure 8 illustrates the effects of the condensation temperature on the MkW values of both systems, ORC-VCRC and ORC-EERCIWB, $MkW_{(ORC–VCRC)}$ and $MkW_{(ORC–EERCIWB)}$, respectively, using the hydrocarbon R600a as a working fluid.

It is evident that as the condensation temperature rises, the MkW of both systems increase. Figure 8 makes it clear that for the ORC-VCR and ORC-EERCIWB systems, a lower condensation temperature (30°C) resulted in a lower value for the $MkW_{(ORC–VCRC)}$ and $MkW_{(ORC–EERCIWB)}$; on the other hand, a higher condensation temperature (55°C) resulted in a higher value for the $MkW_{(ORC–VCRC)}$ and $MkW_{(ORC–EERCIWB)}$. When the condensation temperature rises from 30°C to 55°C, the MkW values of the two systems using the hydrocarbon R600a increase from 0.0070 to 0.0238 and from 0.0047 to 0.0150, respectively, which signifies that the efficiency of both investigated systems is decreasing. The following provides an explanation of the situation's cause. The rise of the condensation temperature forces the compressor units of the investigated systems to consume more power while simultaneously reducing the cooling capacity each kilogram of a refrigerant can provide. Consequently, the MkW increases substantially.

By comparing the results obtained for the hybrid ORC-VCRC system, it is observed that the MkW values of the proposed hybrid ORC-EERCIWB system are lower than those of the ORC-VCRC system across the entire condensation temperature range, and the variations between the values of $MkW_{(ORC–VCRC)}$ and $MkW_{(ORC–EERCIWB)}$ are greater at high condenser temperatures than at low ones. The following provides an explanation of the situation's cause. When the condenser temperature rises, the compressor in the traditional (ORC-VCRC) system is penalised more severely as it must overcome a much larger pressure gap. Consequently, the performance advantage of the novel system is most pronounced under these demanding conditions,

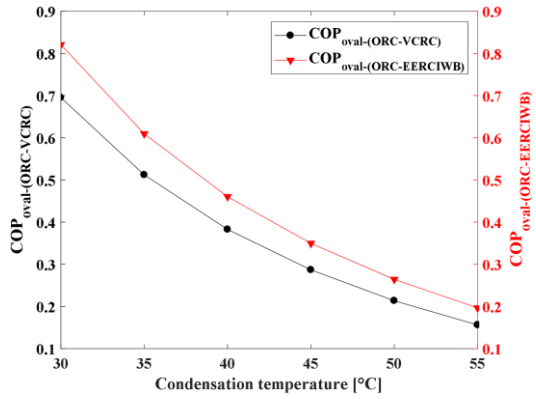

Fig. 7. Effect of condensation temperature on COP_{oval} of the ORC-VCRC and ORC-EERCIWB.

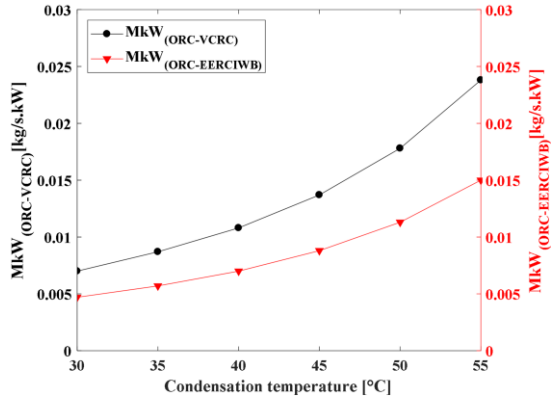

Fig. 8. Effect of condensation temperature on MkW of the ORC-VCRC and ORC-EERCIWB.

where its compressor unit starts at a higher inlet pressure compared to the traditional system, which leads to a sharp decrease in the working fluid mass flow required for each unit of cooling (MkW).

According to the obtained data, the MkW in the ORC-EERCIWB system is lower than in the ORC-VCRC system by 32.85% to 36.97%, leading to a higher COP_{oval}.

Figure 9 depicts the evolution of EPR as a function of condensation temperature for both systems (ORC-VCRC and ORC-EERCIWB) using the hydrocarbon R600a as a working fluid. It is clear that when the condensation temperature rises, the EPR decreases. The reason for this behaviour is that a higher condenser temperature forces a higher condensation pressure. Consequently, the expander unit faces a higher outlet pressure while its inlet pressure, which is set by the boiler temperature, is unchanged. This reduced pressure difference across the expander unit results in a smaller expansion in the volume of the working fluid, which directly leads to a lower EPR for the investigated systems. The EPR values for both systems increase from 3.6239 to 1.8586 as the condensation temperature rises from 30 to 55°C.

Figure 10 shows the impact of changes in condensation temperatures on the CMR values of the ORC-VCRC and ORC-EERCIWB combined refrigeration and power systems, $CMR_{(ORC–VCRC)}$ and $CMR_{(ORC–EERCIWB)}$, respectively. The figure indicates that both $CMR_{(ORC–VCRC)}$ and $CMR_{(ORC–EERCIWB)}$ increase as the condenser temperature rises. This is because the compressor's discharge pressure in the investigated systems is determined by the condensing temperature. As the condensation temperature rises, the pressure the compressor must push against significantly increases. On the other hand, the pressure at the inlet of the compressor remains constant. Because of these two effects, the compressors of the investigated systems have to raise the gas from a fixed suction pressure to a much higher discharge pressure. As a result, the CMR increases substantially. This places a greater thermodynamic load on the compressors of the investigated systems, reducing their efficiency. The CMR values obtained for both systems using the R600a increase from 2.1675 to 4.1398 and from 1.3785 to 2.4205, respectively, as the condensation temperature increases from 30°C to 55°C. It is also noticeable

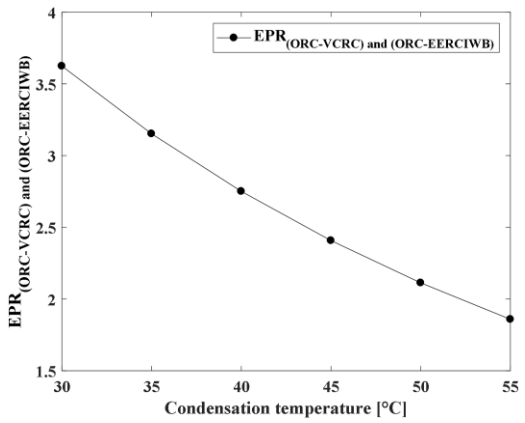

Fig. 9. Effect of condensation temperature on EPR in the ORC-VCRC and ORC-EERCIWB.

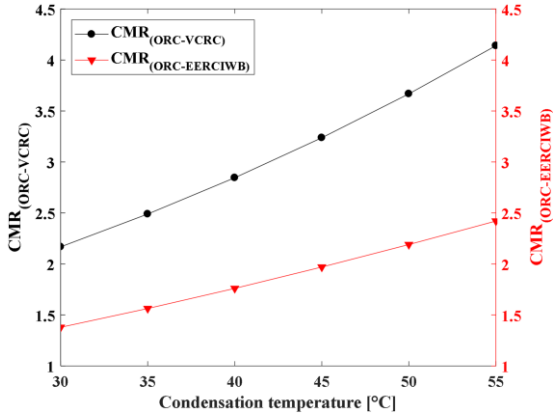

Fig. 10. Effect of condensation temperature on CMR in the ORC-VCRC and ORC-EERCIWB.

that the minimum $CMR_{(ORC–VCRC)}$ and $CMR_{(ORC–EERCIWB)}$ are attained at 30°C, but the maximum $CMR_{(ORC–VCRC)}$ are at 55°C.

Upon comparing the results obtained for the two systems, it can be observed that the ORC-VCRC system achieves the maximum CMR, while the proposed ORC-EERCIWB system achieves the minimum CMR. The new system has a lower MkW because its compressor unit starts at a higher inlet pressure, precompressed by the booster unit and ejector device. This proposed architecture results in a much lower compression ratio. Specifically, the CMR in the ORC-EERCIWB system is reduced by 36.40% to 41.53% compared to the ORC-VCRC system.

4.3. Effect of evaporation temperature on performance indicators

The following Figs. 11–14 show the impact of evaporation temperature on the ORC-VCRC and ORC-EERCIWB performances using the hydrocarbon R600a as a working fluid, while maintaining the other parameters constant (T_{boil} = 80°C, T_{cond} = 40°C).

The effects of the evaporation temperature on the COP_{oval} of the two systems, ORC-VCRC and ORC-EERCIWB, respectively, are displayed in Fig.11. According to the figure, the simulation results demonstrate that the evaporation temperature has

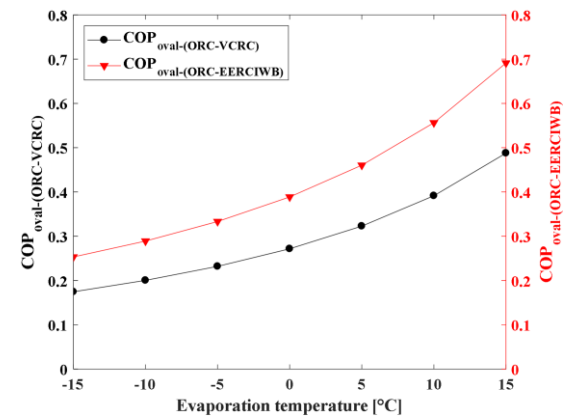

Fig. 11. Effect of evaporation temperature on COP_{oval} of the ORC-VCRC and ORC-EERCIWB.

a significant impact on the overall COP of both systems. Specifically, increasing the evaporation temperature significantly increases the COP_{ovals} of both systems. This, in turn, improves the overall COP of the combined refrigeration and power systems. An increase in temperature within the system's evaporator leads to an improvement in cooling capacity due to the resulting increase in the refrigeration effect. Both effects boost the overall COP of the systems, ORC-VCRC and ORC-EERCIWB. As the evaporation temperature reaches 15°C, the COP of the two systems, i.e. $COP_{oval\text{-}(ORC–VCRC)}$ and $COP_{oval\text{-}(ORC–EERCIWB)}$, increases, as shown in Fig.11. The COP_{oval} obtained with the hydrocarbon R600a in the ORC-VCRC system and ORC-EERCIWB system is 0.4877 and 0.6912, respectively. It should be noted that as the evaporation temperature rises from –15°C to 15°C, the determined COP_{oval} values of the two systems rise from 0.1745 to 0.4877 and 0.2532 to 0.6912, respectively.

When the overall COP of the two systems are compared, it is observed that the ORC-EERCIWB system is the most efficient, where the ORC-EERCIWB system reveals the highest COP_{oval} values by 45.10% to 41.72% than that in the ORC-VCRC system. This improvement is due to a gain in refrigeration in the ORC-EERCIWB system compared to the ORC–VCRC system.

Figure 12 shows how the evaporation temperature affects the MkW for R600a in the ORC-VCRC and ORC-EERCIWB systems. It is evident from the graphs that the MkW of both systems decreases, which signifies that the refrigeration of both investigated systems becomes fundamentally more efficient with the rise of the evaporation temperature. This variation can be explained by the fact that, as the evaporator temperature rises, a higher evaporator pressure reduces the compressor's workload in the investigated systems, allowing it to circulate more mass flow of a working fluid using the same power input for both systems. Simultaneously, the amount of cooling each kilogram of the working fluid can provide increases. This results in the cooling capacity growing much faster than the working fluid mass flow rate, causing the mass flow per unit of cooling to fall. When the evaporation temperature rises from –15°C to 15°C, the MkW values of the two systems, ORC-VCRC and ORC-EERCIWB, decrease from 0.0227 to 0.0102 and from 0.0119 to 0.0051, respectively.

Comparing the MkW simulation results for the two systems, it is found that the ORC-VCRC system achieves the maximum MkW, while the proposed ORC-EERCIWB system achieves the minimum MkW. This can be explained by the fact that for the same cooling power output, the proposed (ORC-EERCIWB) system requires a lower mass flow rate of refrigerant than the traditional (ORC-VCRC) system. The MkW in the ORC-EERCIWB system is lower than that of the ORC-VCRC system by 47.6% (at lower evaporation temperature) to 50% (at higher evaporation temperature), and the differences between the values of $MkW_{(ORC–VCRC)}$ and $MkW_{(ORC–EERCIWB)}$ are greater at low evaporation temperatures than they are at high evaporation temperatures.

Figure 13 represents the effect of the evaporation temperature on the CMR of the combined refrigeration and power systems, ORC-VCR and ORC-EERCIWB, respectively, using R600a as a working fluid. It is observed from the figure that the two curves of $CMR_{(ORC–VCRC)}$ and $CMR_{(ORC–EERCIWB)}$ decrease with an increase in evaporation temperature. This is justified as the temperature and pressure are kept constant at the outlet of the compressors of both systems, and an increase in the evaporation temperature causes the rise of pressure and enthalpy at the inlet of the compressor, which leads to the decrease in CMR of both systems as the evaporation temperature rises. The figure also shows that when the evaporation temperature rises from –15°C to 15°C, the CMR values for the two investigated systems using the R600a increase from 5.9651 to 2.0511 and from 3.3708 to 1.3056, respectively.

When the results for the two systems are compared, it can be seen that the ORC-VCRC system achieves the maximum CMR, while the proposed ORC–EERCIWB system achieves the minimum CMR. This difference can be explained as follows: The compressor unit of the traditional system (ORC-VCRC) must raise pressure from the very low evaporator pressure all the way up to the condenser pressure. In contrast, the investigated new (ORC-EERCIWB) system uses a booster unit and an ejector device to compress the working fluid before it reaches the main compressor unit of the proposed system. The booster unit elevates the pressure from the evaporator unit to a higher intermediate pressure, and the ejector device further increases it. Therefore, the main compressor unit in the proposed system starts

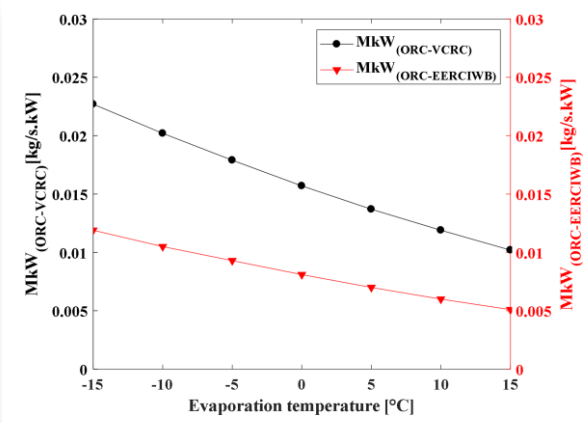

Fig. 12. Effect of evaporation temperature on MkW in the ORC-VCR and ORC-EERCIWB.

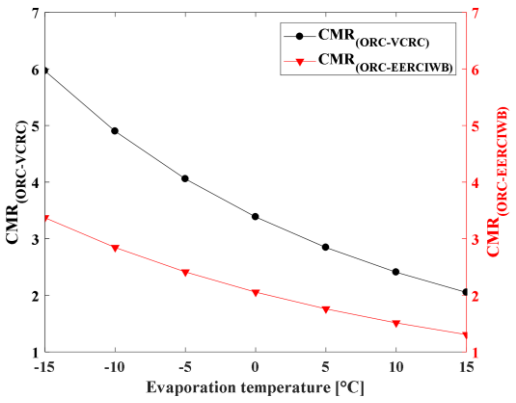

Fig. 13. Effect of evaporation temperature on CMR in the ORC–VCRC and ORC–EERCIWB.

from a significantly higher inlet pressure, resulting in a much lower and more efficient CMR. The CMR in the ORC-EERCIWB system is lower than that of the ORC-VCRC system by 43.49% to 36.34%, and the differences in values between $CMR_{(ORC–VCRC)}$ and $CMR_{(ORC–EERCIWB)}$ are greater at low evaporation temperatures than they are at high evaporation temperatures.

5. Conclusions

In the present work, a unique setup for a combined power-cooling (ORC–EERCIWB) system that is activated by low-grade thermal energy is proposed and investigated.

The preferred architecture for the power-cooling system is a combined organic Rankine cycle (ORC) and an ejector-expansion refrigeration cycle that improves with a booster (EERCIWB) unit.

The suggested system employs the R600a as a working fluid. The energy analysis is performed to analyse the suggested system's performance indicators by comparing it to the classic power-cooling (ORC-VCRC) system, which is widely utilised, under the same operating conditions. Furthermore, an analysis and discussion are undertaken on the impact of operational factors, notably the boiler, condensation and evaporation temperatures, on the performance indicators of the ORC-EERCIWB and ORC-VCRC power-cooling systems.

The energy analysis and comparison of the ORC-EERCIWB and ORC-VCRC systems were carried out at temperatures ranging from 60°C to 90°C for the boiler, 30°C to 55°C for condensation and −15°C to 15°C for evaporation.

The simulation results include the following performance indicators: cooling capacity, expansion ratio, compression ratio and overall coefficient of performance.

Overall, the numerical findings show that the ORC-EERCIWB system outperformed the ORC-VCRC system in terms of performance. Furthermore, the three thermodynamic parameters, the boiler, condensation and evaporation temperatures, have a considerable impact on both systems' expansion ratio, compression ratio and performance indicators.

Based on the obtained results for the examined configurations (ORC-VCRC and ORC-EERCIWB), the following concluding remarks have been set:

- The thermodynamic performances of both systems are significantly influenced by the temperatures of the boiler, condenser and evaporator.
- For the two systems under investigation, when both the boiler temperature and the evaporation temperature rise, the overall coefficient of performance rises, and the working fluid mass flow rate per kW of cooling capacity falls.
- As the condensation temperature rises, the overall coefficient of performance for the two systems examined decreases, and the working fluid mass flow rate per kW of cooling capacity rises.
- The expansion ratio in the expander for the two systems under study rises as the boiler temperature rises and falls as the condensation temperature rises.
- The compression ratio in the compressor for the two systems under investigation increases as the condensation temperature rises and falls as the evaporation temperature rises.
- Boiler temperature was the most crucial variable for both systems, followed by evaporator and condenser temperatures.
- When the same operating conditions are taken into account, the ORC-EERCIWB system performs better overall than the ORC-VCRC system and has a lower working fluid mass flow rate per kW of cooling capacity, as well as a compression ratio in the compressor.
- At a boiler exit temperature of 90°C, the maximum coefficient of performance values for both systems were found to be 0.5385 and 0.4476, respectively; the value of the ORC-EERCIWB system increased by 20.30% compared to that of the ORC-VCRC system.
- At a boiler exit temperature of 90°C, the minimum working fluid mass flow rates per kW of cooling capacity were found to be 0.0064 and 0.0096, respectively, where the value of ORC-EERCIWB dropped by 33.33% compared to ORC-VCRC.
- At an evaporation temperature of 15°C, the maximum coefficient of performance values for both systems were found to be 0.6912 and 0.4877, respectively; the value of the ORC-EERCIWB system increased by 41.72% compared to the ORC-VCRC system.
- For an evaporation temperature of 15°C, the minimum working fluid mass flow rates per kW of cooling capacity of the two systems were found to be 0.0051 and 0.0102, respectively, with the value of the ORC-EERCIWB system decreased by 50% compared to that of the ORC-VCRC system.

The study's findings promote future research on unique configurations of combined power-cooling utilisation that incorporate the two-phase ejector-expander in cooling cycles. Based on the findings, it can be concluded that the usage of the EERCIWB, which is meant to be utilised for combined power-cooling systems and is commonly used to replace VCRC in standard combined power-cooling systems, is effective.

References

[1] Hung, T.C., Wang, S.K., Kuo, C.H., Pei, B.S., & Tsai, K.F. (2010). A study of organic working fluids on system efficiency of an ORC using low-grade energy sources. *Energy*, 35(3), 1403–1411. doi: 10.1016/j.energy.2009.11.025

[2] Drescher, U., & Brüggemann, D. (2007). Fluid selection for the Organic Rankine Cycle (ORC) in biomass power and heat plants. *Applied Thermal Engineering*, 27(1), 223–228. doi: 10.1016/j.applthermaleng.2006.04.024

[3] Guo, C., Du, X., Yang, L., & Yang, Y. (2014). Performance analysis of organic Rankine cycle based on location of heat transfer pinch point in evaporator. *Applied Thermal Engineering*, 62(1), 176–186. doi: 10.1016/j.applthermaleng.2013.09.036

[4] Rafique, M.M. (2020). Evaluation of metal–organic frameworks as potential adsorbents for solar cooling applications. *Applied System Innovation*, 3(2), 26. doi: 10.3390/asi3020026

[5] Bellos, E., & Tzivanidis, C. (2020). Financial optimization of a solar-driven organic Rankine cycle. *Applied System Innovation*, 3(2), 23. doi: 10.3390/asi3020023

[6] Deng, J., Wang, R.Z., & Han, G.Y. (2011). A review of thermally activated cooling technologies for combined cooling, heating and power systems. *Progress in Energy and Combustion Science*, 37(2), 172–203. doi: 10.1016/j.pecs.2010.05.003

[7] Wang, H., Peterson, R., & Herron, T. (2011). Design study of configurations on system COP for a combined ORC (organic Rankine cycle) and VCC (vapor compression cycle). *Energy*, 36(8), 4809–4820. doi: 10.1016/j.energy.2011.05.015

[8] Pektezel, O., & Acar, H.I. (2019). Energy and exergy analysis of combined organic Rankine cycle-single and dual evaporator vapor compression refrigeration cycle. *Applied Sciences*, 9(23), 5028. doi: 10.3390/app9235028

[9] Sun, W., Yue, X., & Wang, Y. (2017). Exergy efficiency analysis of ORC (Organic Rankine Cycle) and ORC-based combined cycles driven by low-temperature waste heat. *Energy Conversion and Management*, 135, 63–73. doi: 10.1016/j.enconman.2016.12.042

[10] Xu, F., Goswami, D.Y., & Bhagwat, S.S. (2000). A combined power/cooling cycle. *Energy*, 25(3), 233–246. doi: 10.1016/S0360-5442(99)00071-7

[11] Zhang, N., & Lior, N. (2007). Methodology for thermal design of novel combined refrigeration/power binary fluid systems. *International Journal of Refrigeration*, 30(6), 1072–1085. doi: 10.1016/j.ijrefrig.2006.12.005

[12] Vijayaraghavan, S., Goswami, D.Y. (2003). On evaluating efficiency of a combined power and cooling cycle. *Journal of Energy Resources Technology*, 125(3), 221–227. doi:10.1115/1.1595110.

[13] Aphornratanaa, S., & Sriveerakul, T. (2011). Analysis of a combined Rankine–vapour–compression refrigeration cycle. *Energy Conversion and Management*, 51(12), 2557–2564. doi: 10.1016/j.enconman.2010.04.016

[14] Molés, F., Navarro-Esbrí, J., Peris, B., Mota-Babiloni, A., & Kontomaris, K. (2015). Thermodynamic analysis of a combined organic Rankine cycle and vapor compression cycle system activated with low temperature heat sources using low GWP fluids. *Applied Thermal Engineering*. 87, 444–453. doi: 10.1016/j.applthermaleng.2015.04.083

[15] Li, H., Bu, X., Wang, L., Long, Z., & Lian, Y. (2013). Hydrocarbon working fluids for a Rankine cycle powered vapor compression refrigeration system using low-grade thermal energy. *Energy and Buildings*, 65, 167–172. doi: 10.1016/j.enbuild.2013.06.012

[16] Asim, M., Leung, M.K.H., Shan, Z., Li, Y., Leung, D.Y.C., & Ni, M. (2017). Thermodynamic and Thermo-economic Analysis of Integrated Organic Rankine Cycle for Waste Heat Recovery from Vapor Compression Refrigeration Cycle. *Energy Procedia*, 143, 192–198. doi: 10.1016/j.egypro.2017.12.670

[17] Saleh, B. (2016). Parametric and working fluid analysis of a combined organic Rankine-vapor compression refrigeration system activated by low-grade thermal energy. *Journal of Advanced Research*, 7(5), 651–660. doi: 10.1016/j.jare.2016.06.006

[18] Lizarte, R., Palacios-Lorenzo, M.E., & Marcos, J.D. (2017). Parametric study of a novel organic Rankine cycle combined with a cascade refrigeration cycle (ORC-CRS) using natural refrigerants. *Applied Thermal Engineering*, 127, 378–389. doi: 10.1016/j.applthermaleng.2017.08.063

[19] Cihan, E. (2014). Cooling Performance Investigation of a System with an Organic Rankine Cycle Using Waste Heat Sources. *Journal of Thermal Science and Technology*, 34(1), 101–109. https://dergipark.org.tr/en/pub/isibted/issue/33968/375961 (in Turkish)

[20] Bu, X., Wang, L., & Li, H. (2013). Performance analysis and working fluid selection for geothermal energy-powered organic Rankine-vapor compression air conditioning. *Geothermal Energy*, 1, 2. doi: 10.1186/2195-9706-1-2

[21] Wang, H., Peterson, R., Harada, K., Miller, E., Ingram-Goble, R., Fisher, L., Yih, J., & Ward, C. (2011). Performance of a combined organic Rankine cycle and vapor compression cycle for heat activated cooling. *Energy*, 36(1), 447–458. doi: 10.1016/j.energy.2010.10.020

[22] Yue, C., You, F., & Huang, Y. (2016). Thermal and economic analysis of an energy system of an ORC coupled with vehicle air conditioning. *International Journal of Refrigeration*, 64, 152–167. doi: 10.1016/j.ijrefrig.2016.01.005

[23] Hu, B., Guo, J., Yang, Y., & Shao, Y. (2022). Performance analysis and working fluid selection of organic Rankine steam compression air conditioning driven by ship waste heat. *Energy Reports*, 8(S3), 194–202. doi: 10.1016/j.egyr.2022.01.094.

[24] Khatoon, S., Almefreji, N.M.A., & Kim, M.H. (2021). Thermodynamic study of a combined power and refrigeration system for low-grade heat energy source. *Energies*, 14(2), 410. doi: 10.3390/en14020410

[25] Kim, K.H., & Perez-Blanco, H. (2015). Performance analysis of a combined organic Rankine cycle and vapor compression cycle for power and refrigeration cogeneration. *Applied Thermal Engineering*, 91, 964–974. doi: 10.1016/j.applthermaleng.2015.04.062

[26] Jeong, J., & Kang, Y.T. (2004). Cycle of a refrigeration cycle driven by refrigerant steam turbine. *International Journal of Refrigeration*, 27(1), 33–41. doi:10.1016/S0140-7007(03)00101-4.

[27] Egrican, A.N., & Karakas, A. (1986). Second law analysis of a solar powered Rankine cycle/vapor compression cycle. *Journal of Heat Recovery Systems*, 6(2), 135–141. doi: 10.1016/0198-7593(86)90073-1

[28] González, J., Llovell, F., Matías Garrido, J., & Quinteros-Lama, H. (2023). A study of the optimal conditions for organic Rankine cycles coupled with vapour compression refrigeration using a rigorous approach based on the Helmholtz energy function. *Energy*, 285, 129554. doi: 10.1016/j.energy.2023.129554

[29] Wu, D., Hu, B., & Wang, R.Z. (2021). Vapor compression heat pumps with pure Low-GWP refrigerants. *Renewable and Sustainable Energy Reviews*, 138, 110571. doi: 10.1016/j.rser.2020.110571

[30] Maalem, Y., & Madani, H. (2025). Performance Characteristics Investigation of a Solar Rankine Cycle Powered Air Conditioning System for Residential Buildings using Low GWP Working Fluids. *Archives of Thermodynamics*, 46(1), 97–107. doi: 10.24425/ather.2025.154184

[31] Elbel, S., & Lawrence, N. (2016). Review of recent developments in advanced ejector technology. *International Journal of Refrigeration*, 62, 1–18. doi: 10.1016/j.ijrefrig.2015.10.031

[32] Chen, X., Omer, S., Worall, M., & Riffat, S. (2013). Recent developments in ejector refrigeration technologies. *Renewable and Sustainable Energy Reviews*, 19, 629–651. doi: 10.1016/j.rser.2012.11.028

[33] Hacipaşaoğlu, S.G., & Öztürk, I. (2023). Energy and exergy analysis in the ejector expansion refrigeration cycle under optimum conditions. *International Advanced Researches and Engineering Journal*, 7(1), 23–34. doi: 10.35860/iarej.1171637

[34] Maalem, Y., Fedali, S., Madani, H., & Tamene, Y. (2020). Performance analysis of ternary azeotropic mixtures in different vapor compression refrigeration cycles. *International Journal of Refrigeration*, 119, 139–151. doi: 10.1016/j.ijrefrig.2020.07.021

[35] Leila, B., Fedali, S., Bougriou, C., & Madani, H. (2022). Influence of azeotropic binary mixtures on single-stage refrigeration system performance. *High Temperatures–High Pressures*, 51(4), 319–339. doi: 10.32908/hthp.v51.1185

[36] Maalem, Y., Tamene, Y., & Madani, H. (2023). Performances Investigation of the Eco-friendly Refrigerant R13I1 used as Working Fluid in the Ejector-Expansion Refrigeration Cycle. *International Journal of Thermodynamics*, 26(3), 25–35. doi: 10.5541/ijot.1263939

[37] Mehemmai, M., Grine, H., Madani, H., & Bougriou, C. (2023). Performance analysis of ejector refrigeration cycle with zeotropic mixtures. *International Journal of Thermofluid Science and Technology*, 10(4), 100404. doi: 10.36963/IJTST.2023100404

[38] Abdou, C., Madani, H., & Hasseine, A. (2023). Study of the performances of an ejector refrigeration cycle using CO2-based mixtures in subcritical and transcritical mode. *International Journal of Thermofluid Science and Technology*, 10(3), 100304. doi: 10.36963/IJTST.2023100304

[39] Maalem, Y., & Madani, H. (2024). Energetic performance investigation of ejector air conditioning cycles using the environment friendly gas R161 (Fluoroethane) as substitute to the phase-out R22 (Chlorodifluoromethane). *International Journal of Thermofluid Science and Technology*, 11(2), 110201. doi: 10.36963/IJTST.2024110201

[40] Maalem, Y., Boulebbina. C, & Madani, H. (2025). Enhancement of the capabilities of energy and exergy efficiencies of low cascade cooling process. *International Journal of Ambient Energy*, 46(1), 2574415. doi: 10.1080/01430750.2025.2574415

[41] Rostamnejad Takleh, H., & Zare, V. (2019). Performance improvement of ejector expansion refrigeration cycles employing a booster compressor using different refrigerants: Thermodynamic analysis and optimization. *International Journal of Refrigeration*, 101, 56–70. doi: 10.1016/j.ijrefrig.2019.02.031

[42] Liang, Y., Yu, Z., & Li, W. (2019). A waste heat-driven cooling system based on combined organic Rankine and vapour compression refrigeration cycles. *Applied Sciences*, 9(20), 4242. doi: 10.3390/app9204242

[43] Sumeru, K., Nasution, H., & Ani, F.N. (2012). A review on two-phase ejector as an expansion device in vapor compression refrigeration cycle. *Renewable and Sustainable Energy Reviews*, 16(7), 4927–4937. doi: 10.1016/j.rser.2012.04.058

[44] Maalem, Y., & Madani, H. (2025). Performance investigation of an automotive hybrid air-conditioning system without and with an internal heat exchanger (IHX) using R1234ze (E) as substitute for R134a. *International Journal of Automotive Science and Technology*, 9(2), 194–207. doi: 10.30939/ijastech.1594100